Applied Surface Science 283 (2013) 648–653

Contents lists available at SciVerse ScienceDirect

Applied Surface Science

journal homepage: www.elsevier.com/locate/apsusc

Fundamentals of layered nanoparticle covered pyramidal structures formed on nickel during femtosecond laser surface interactions

Craig A. Zuhlke*, Troy P. Anderson, Dennis R. Alexander

Department of Electrical Engineering, University of Nebraska-Lincoln, 844N 16th St, Lincoln, Nebraska 68588, United States

ARTICLE INFO

Article history:
Received 1 May 2013
Received in revised form 28 June 2013
Accepted 1 July 2013
Available online 9 July 2013

Keywords:
Femtosecond phenomena
Laser processing
Microstructuring
Nanostructuring

ABSTRACT

The formation of nanoparticle covered pyramidal structures using femtosecond laser pulses with a fluence near the ablation threshold is reported for the first time. These unique structures form through a combination of preferential ablation of flat regions around the pyramids and redeposition of nanoparticles created during the ablation process. The structures are demonstrated on nickel and stainless steel 316. When produced by rastering Gaussian pulses across the sample, layers of nanoparticles join together by sintering to form unique layered shells.

1. Introduction

Femtosecond laser surface processing (FLSP) is a rapidly developing technology that can be utilized for creating specialized micro/nanostructures on the surface of various types of materials. The wide range of and precise control over the surface morphologies enable precise tailoring for specific applications. A large variety of micro/nanostructured morphologies fabricated by FLSP have been reported in the literature, including pillars [1–5], cones [6–11] spikes [3,12–14], and mounds [15]. All of these surface morphologies share similar characteristics, namely microstructures with a height to width aspect ratio of at least 2:1, widths around 2–10 μm, and either nanoripples or nanoparticles covering the surface. In this work, we present for the first time a new surface morphology fabricated via FLSP that is referred to as nanoparticle covered pyramids (NC-pyramids). NC-pyramids have a pyramidal shape and are covered with a thick layer of nanoparticles (typically >2 μm thick). The NC-pyramids have an aspect ratio near 1:1 and can grow to be more than 50 μm in height and width. In a recent publication covering FLSP, we demonstrated that different values of the laser fluence lead to dissimilar formation processes for mound-shaped structure growth and therefore unique surface morphologies [15]. NC-pyramids are another unique surface morphology that result from using FLSP at much lower fluences (near the ablation threshold of the material). NC-pyramids form through a series of different processes than either of the mound structures previously reported [15].

The pyramids discussed in this paper are similar in formation and shape to pyramids formed during ion beam bombarded copper [16], as well as through nanosecond laser machining of polymers [17–19] and graphite [20]. As reported in this previous work, the onset of formation occurs when a small portion of the surface has a higher ablation threshold than the surrounding regions, and thus results in preferential ablation along with the subsequent formation of a precursor cone. The existence of regions with increased ablation thresholds is attributed to impurities that are either originally present in the material or deposited during the ablation process. A unique aspect of the pyramidal structures formed using FLSP that is not present through other methods is a thick layer of nanoparticles that builds up on the surface. As a result, the NC-pyramids discussed here appear to be formed as a hybrid structure type that lies between the pyramids formed during nanosecond ablation and the nanoparticle aggregates discussed in one of our earlier publications [21]. One advantage of using FLSP for the formation of NC-pyramidal structures is the minimized heat affected zone [22]. Thus, using FLSP to produce NC-pyramids is an improvement over the use of longer pulsed lasers for applications where the bulk material needs to remain unaltered. This is the first demonstration, to our knowledge, of the formation of NC-pyramidal structures formed on a metal surface using FLSP.

* Corresponding author at: SEC 209N, 844 Nth 16th St., Lincoln, NE 68588, United States. Tel.: +1 402 649 7456.
E-mail addresses: czuhlke11@gmail.com, craig.zuhlke11@huskers.unl.edu (C.A. Zuhlke), troy.anderson@unl.edu (T.P. Anderson), dalexander1@unl.edu (D.R. Alexander).

0169-4332/$ – see front matter © 2013 Elsevier B.V. All rights reserved.
http://dx.doi.org/10.1016/j.apsusc.2013.07.002

2. Experiment

NC-pyramids were produced through two techniques: stationary ablation of the sample using pulses with a square flat-top beam profile and by rastering pulses with a Gaussian-shaped beam profile across the sample surface. The multipulse growth mechanisms of NC-pyramids on nickel using stationary ablation were studied using a stop-motion scanning electron microscopy (SEM) technique similar to that described in our previous publication [15]. Using this technique, a single area on the sample was alternately irradiated and imaged in order to produce a series of high-resolution SEM images that depict the formation processes of individual NC-pyramids with increasing pulse count. These still frame images were sequenced to form high resolution stop-motion SEM videos. The NC-pyramid formation processes occur gradually over 1,000–20,000 pulses. Therefore, the number of pulses between SEM imaging was varied to balance the time commitment and the step size over which interesting results could be observed. The redeposition of ablated nanoparticles on the surface of the pyramids was investigated using both stationary flat-top pulses and rastered Gaussian-shaped pulses in order to isolate the impact of sample motion during processing. The stop-motion imaging work presented here was performed on nickel, which was chosen because of its potential use as electrodes in pseudocapacitor and electrolysis systems, its purity, and the volume of published work on femtosecond pulse interactions with nickel. Similar NC-pyramids have been fabricated via FLSP on stainless steel (SS) (type 316, 304, and 430) in our laboratory. Results on 316 SS are also included.

The laser used for carrying out this research was a Spectra Physics Spitfire, Ti:Sapphire femtosecond laser system capable of producing 1 mJ, 50 fs pulses. In combination with a computer-controlled shutter, the repetition rate of the laser was adjustable from single pulses up to the maximum of 1 kHz. The pulse length and chirp were monitored using a Frequency Resolved Optical Gating (FROG) instrument from Positive Light (Model 8-02). The position of the sample with respect to the laser focal volume was controlled using computer-guided Melles Griot nanomotion translation stages with 3 axes of motion. The laser power was controlled using a half waveplate and a polarizer. All of the work was completed in open atmosphere.

In our previous publication, we demonstrated that the growth of self-organized surface structures is critically dependent on the laser fluence [15]. For this reason, a square-shaped flat-top beam was used for the stop-motion SEM experiments in order to generate a uniform laser fluence on the material surface. The experimental setup and beam profile can be seen in our previous publication [15]. This beam profile was created using a refractive beam shaper from Eksma Optics (GTH-4-2.2FA). The laser fluence varied by less than 20% across the central portion of the beam, and any fluence fluctuations in the flat-top distribution are attributed to the asymmetries and inhomogeneity of the input beam. The flat-top profile is constant over the 50 μm ablation depths studied in this work. The spot size on the sample was determined using the same techniques as described in our previous publication [15]. The impact of sample motion during processing, which is necessary for the fabrication of large structured areas, was investigated by translating the sample through the path of the laser in a rastering pattern. For this portion of the research, the laser had a Gaussian beam profile with an ablation diameter of 600 μm, which was achieved by removing the Gauss-to-top hat beam shaper, 500 mm focal length lens, and beam expander/collimator from the setup described in our previous publication [15].

3. Results

3.1. Shot by shot growth

NC-pyramids form on nickel at laser fluence values in the range of 0.09–0.17 J/cm^2, which is near the 0.05 J/cm^2 ablation threshold for nickel when measured with 300 fs pulses centered at 527 nm [23]. Utilizing stop-motion SEM techniques, the shot-by-shot formation process of the NC-pyramids was analyzed and broken into two growth phases. The first phase is the formation of precursor cones. The second phase is described in two parts occurring concurrently: continued growth of the pyramidal structure on the surface, and the development of the nanoparticle layer. The shot-by-shot growth experiments were completed using a constant laser fluence of 0.12 J/cm^2, and are demonstrated in the stop-motion video (multimedia online: media 1) and a sequence of images from this video in Fig. 1. It is highly recommended to view the stop-motion video (multimedia online: media 1) in addition to viewing the images in Fig. 1 in order to be in a position to most readily understand the intricacies of the formation dynamics. These SEM videos provide a powerful shot-by-shot visualization of the growth of single structures in the ablation region and greatly contribute to the understanding of the dynamics involved in the formation of these structures in time and space.

3.1.1. Phase I: Development of precursor cones

The first phase of NC-pyramid development is the formation of precursor cones over a large number of laser pulses, which occurs at the same time that laser induced periodic surface structures (LIPSS) are produced on the surface. LIPSS from FLSP is well published in the literature, including work on metals [24–26]. These LIPSS lines do not contribute to the formation of the NC-pyramids being reported in this paper. However, LIPSS are present over the entire ablation region before NC-pyramids begin to form, in the flat regions between NC-pyramids throughout the formation process, and even on the surface of the pyramids before the nanoparticle layer fully develops and covers the pyramids (see Fig. 1a and b). With increasing pulse counts, small cones begin to form on the LIPSS covered surface (the first cone appears around 1000 pulses in this sample). Fig. 1a is a SEM image of a cone that has developed by the end of the first phase. As has been previously discussed, these conical structures develop from localized regions with an increased ablation threshold relative to the bulk material. Since NC-pyramids form with laser fluence values near the ablation threshold, any variation in the ablation threshold has a direct impact on the ablation rate. Over many thousands of pulses, the cumulative effect of a variation in the ablation rate is the formation of features tens of microns in size. The source of the initial inhomogeneity that causes the formation of the precursor cone has been previously attributed to impurities on the sample when fabricated with nanosecond pulses. For example, Krajnovich and Vazquez conclude in their work on nanosecond ablation of polymers that the higher ablation threshold is from carbon enrichment [18]. Species are preferentially ejected from the material, leaving behind a carbon rich surface, which has a higher ablation threshold. As a different example, Krajnovich et al. conclude in their work on nanosecond ablation of highly oriented pyrolytic graphite (HOPG), cone formation is initiated by micrometer-sized impurities of Ti, V and Fe. It is suggested that the impurities act as heat sinks, shunting heat away and leading to lower sputtering rates in the localized area [20]. In the case of FLSP, it is believed that sources for localized variations in the ablation threshold include: a localized crystalline structure difference (e.g. grain boundaries), impurities in the sample, or modifications in the material from previous pulses (e.g. redeposition of material ejected during the ablation process, which leads to an

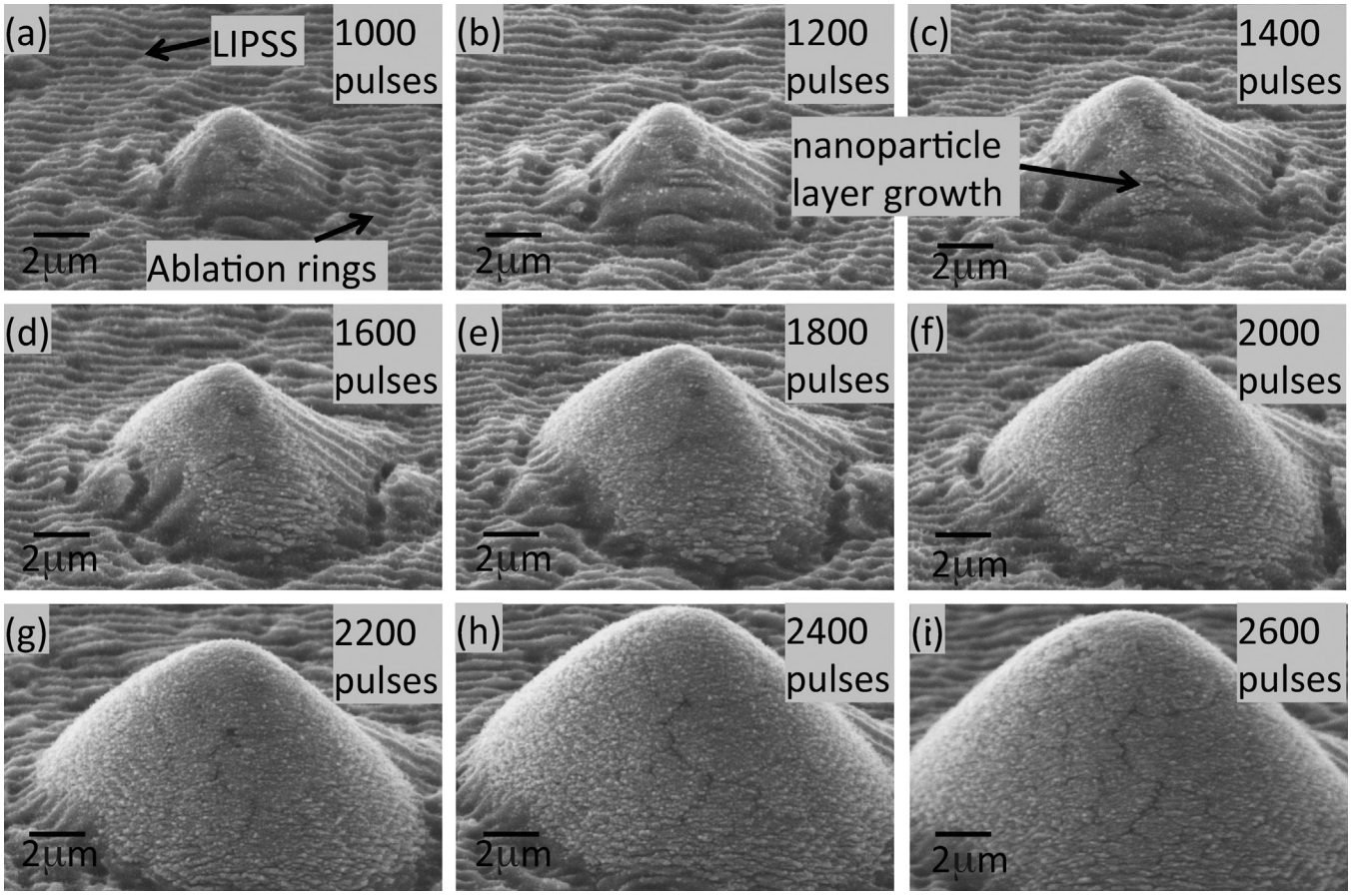

Fig. 1. (multimedia online: media 1). SEM images of stepped NC-pyramid growth from the stop-motion SEM analysis of nickel imaged at 45° after the specified number of pulses. Part (a) represents the end of the first phase. Parts (b)–(i) represent the second phase. These images represent single frames of media 1.

inhomogeneous distribution of absorbed energy from subsequent laser pulses).

It is also interesting to note that the slope of the precursor cone, as it develops in phase I, determines the slope of NC-pyramid structure as it grows throughout phase II. This slope may be attributed to the angular distribution of scattered light from the initial precursor site. Indeed, calculations for Mie scattering of a 2 μm particle (corresponding to the size of the tip of the precursor cone) predict oscillations in the intensity of light as a function of angle; the location of rings seen around the base of precursor cone in Fig. 1a corresponds well to these predictions. This is consistent with an explanation of the formation of similar structures on polymide using nanosecond laser pulses as described by Dyer et al. [17]. Alternatively, in the work by Krajnovich et al. on HOPG, the presence of the metal impurities serves to dissipate heat from the surface and lowering the localized ablation rate of the surrounding material [20]. The slope of the cones is then proportional to the induced variation of the ablation rate around the impurity. Further studies are needed to determine which process significantly impacts the slope of NC-pyramids fabricated via FLSP. Once developed, these cones then act as precursor sites for the preferential ablation process and nanoparticle redeposition that dominates the second phase of the formation.

3.1.2. Phase II-A: Development of pyramid structures

The second phase in the growth of the pyramids is characterized by the progression of the precursor cone, discussed in Phase I, to the final NC-pyramid morphology and is described in two parts: Part A and Part B. Part A describes the development of the micro-scale pyramid structure. With increasing ablation pulse counts, the cone is preferentially ablated into the surface while keeping the same aspect ratio. Preferential ablation is the result of two phenomena: first, a percentage of the light incident on the side of the NC-pyramids is reflected into the flat regions between precursor cones, which increases the total fluence in these areas; second, the portion of the beam incident on the sides of structures is spread over a larger geometric area, which further decreases the fluence relative to the valleys where the pulse is normal to the surface [9,15]. These processes are graphically illustrated in Fig. 2. By analyzing SEM images of pyramids at steep viewing angles, it is estimated that the pyramids have a slope of 55°. At this angle, the fluence will be 42.5% lower on the sides of the pyramids than on the flat regions due to the increased subtended area; this projected area difference

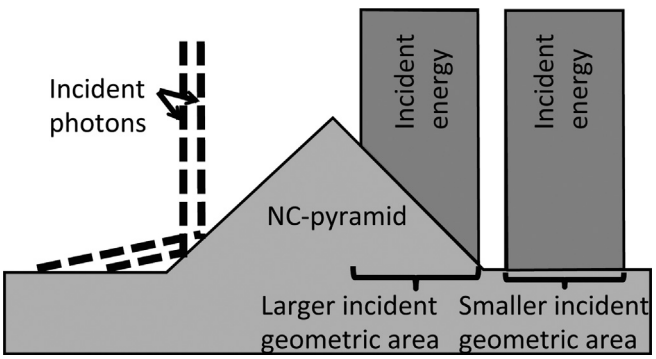

Fig. 2. Diagram of the effect of structure geometry on light distribution that leads to preferential ablation.

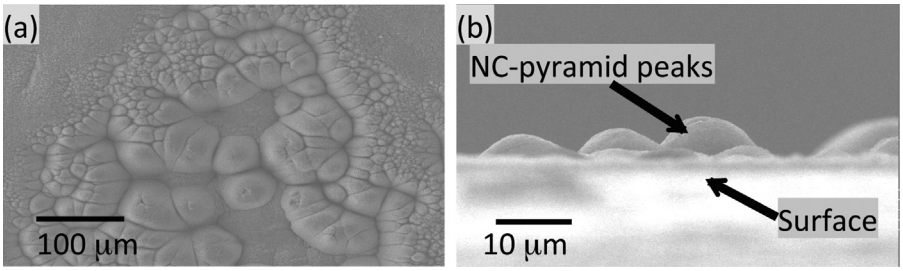

Fig. 3. SEM images of NC-pyramids on 316 SS produced using Gaussian focused pulses with 5000 pulses at 0.16 J/cm^2, viewed at (a) normal incidence (b) 90°.

decreases the laser fluence from 0.12 J/cm^2 down to 0.069 J/cm^2. With laser fluence values so close to the ablation threshold, this reduction in fluence can significantly impact the ablation rates of the NC-pyramids versus the valleys between them. Over thousands of pulses, the combined affect will be perpetuated and lead to the development of the NC-pyramid structures observed.

3.1.3. Phase II-B: Development of the nanoparticle layer on the pyramid structures

Another aspect of the second phase is the onset of nanoparticle redeposition, which occurs at the same time as the pyramid growth due to preferential ablation (Phase II-A). With each incident pulse, the ablation process leads to the ejection of nanoparticles from the surface, some of which subsequently redeposit on the sample surface. The fluence is sufficiently high in the flat regions that each laser pulse ablates any redeposited nanoparticles, which is evident from the presence of LIPSS and the absence of nanoparticles on the flat regions in every image of Fig. 1. However, redeposited nanoparticles are not ablated off of the sides of the NC-pyramids where the fluence is lower. Eventually, the nanoparticles cover the entire NC-pyramid. The gradual development of the nanoparticle layer as it begins to cover the pyramid structure is observable in Fig. 1 in the range of 1000–2000 pulses. Note that the tip of the NC-pyramid also broadens and grows above the original surface with increased shot numbers due to the growth of the nanoparticle layer. This upward growth is even more evident on 316 SS where the peaks of pyramids have been demonstrated to grow above the original surface (see Fig. 3b).

3.1.4. Effect of sample motion during processing on nanoparticle layer development

A common method to produce multiscale surface structures via FLSP over a large area relative to the beam size is to raster the sample through the path of the beam. However, whether or not the sample is in motion during processing impacts the development of the nanoparticle layer in phase II-B of NC-pyramid formation. This impact can be analyzed by placing a processed sample in an ultrasonic bath filled with distilled water to break apart the nanoparticle layer and reveal the internal structure. SEM images of broken NC-pyramids formed by a stationary flat-top and a rastered Gaussian beam are shown in Fig. 4a–d, respectively. For the sample produced by rastering the Gaussian beam profile, the ablation diameter produced from 100 pulses at 0.248 J/cm^2 was 600 μm. The sample was rastered at a speed of 0.8 mm/s with a pitch of 15 μm. This combination of spot size and translation speed results in the sample being irradiated with 750 pulses/area for each rastering pass. With a 15 μm pitch, each area of the sample is irradiated for 40 consecutive rastering passes, resulting in a total of 30,000 pulses/area.

Only a single layer of nanoparticles appears to be present when a sample produced from stationary ablation has been cleaned in the ultrasonic bath (see Fig. 4a and b). However, a series of concentric shells is observed when the sample is produced using a rastered beam. These concentric nanoparticle shells are similar to

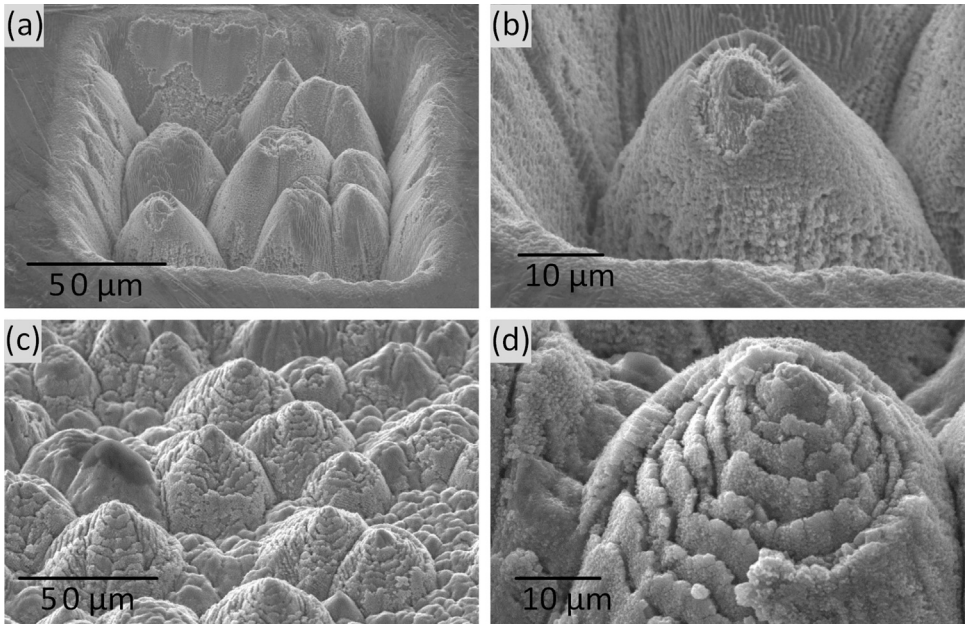

Fig. 4. SEM images of pyramids formed using the following parameters: parts (a) and (b) stationary ablation with the square flat-top profile using 20,000 pulses at 0.12 J/cm^2, after cleaning in an ultrasonic bath. Parts (c) and (d) rastering Gaussian focused pulses with 30,000 pulses/area at 0.248 J/cm^2, after cleaning in an ultrasonic bath.

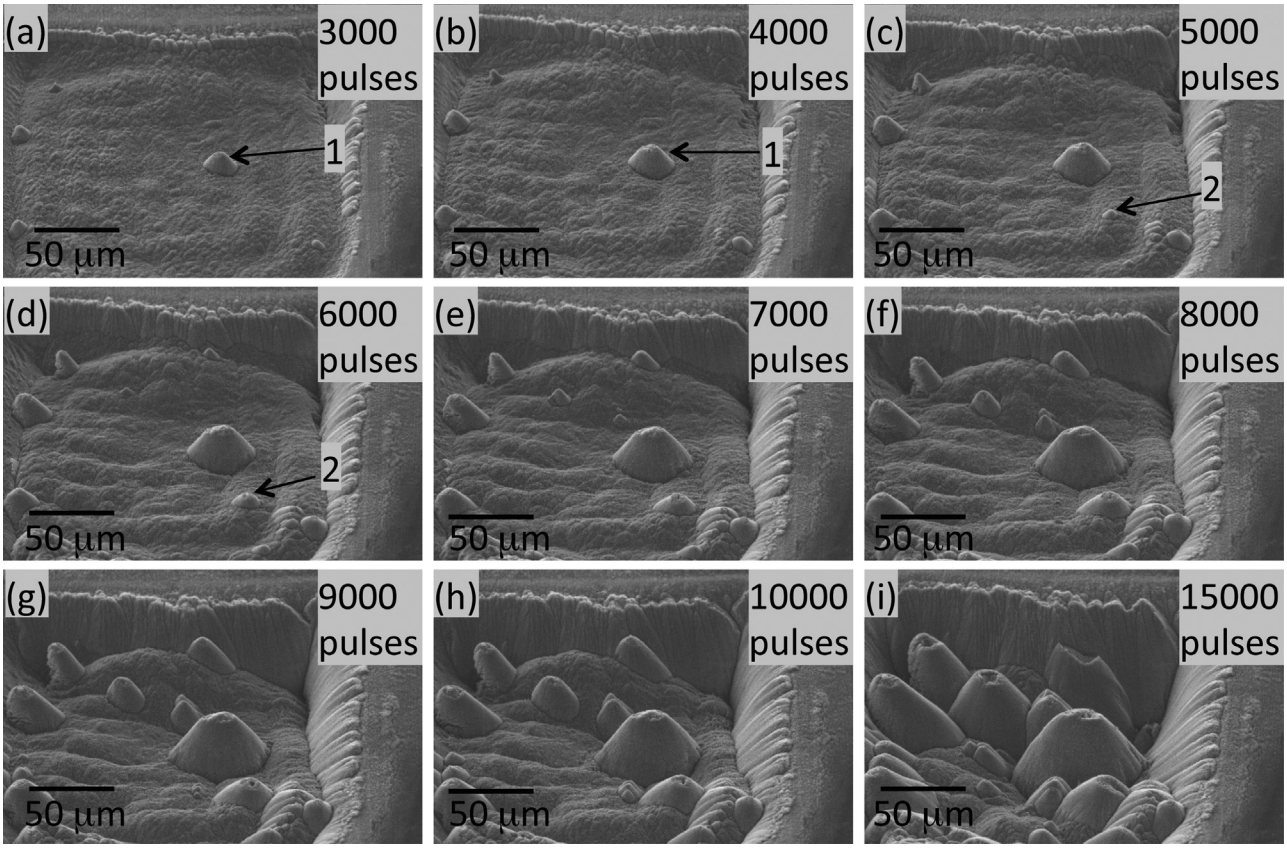

Fig. 5. SEM images of stepped NC-pyramid growth from the stop-motion SEM technique on nickel imaged at 45° after the specified number of pulses.

the nanoparticle aggregates produced on aluminum by Zuhlke et al. [21]. The formation of these shells can be attributed to rastering. Individual shells form when the laser is ablating regions around but not directly over a NC-pyramid and ejected particles land on the pyramid. As the sample is translated so that the laser irradiates the NC-pyramid, the nanoparticle layer that has built up on the pyramid is sintered together as a single layer. This process occurs with each rastering pass, leading to the formation of several shells of nanoparticles. For the sample displayed in Fig. 4c and d, each structure was irradiated with a portion of the pulse profile for 40 consecutive rastering passes. At least nine shells are clearly visible on the NC-pyramid in Fig. 4d. The discrepancy between the number of shells and the number of irradiating rastering passes, can be accounted for by considering that a full shell will only form when the entire structure is irradiated in a single rastering pass. For the pyramid in Fig. 4d, with a 50 μm diameter base, and considering the 600 μm spot size, the entire structure was illuminated for 12 consecutive passes, which explains the lower number of shells. Further discrepancy can be attributed to the Gaussian profile of the focused pulses, which leads to a varying fluence for the portion of the pulse profile incident on the structure for consecutive rastering passes. This varying fluence would also account for variations in shell thicknesses. This same process does not occur with stationary ablation and explains the absence of shell structures in Fig. 4a and b.

3.1.5. Development of multiple NC-pyramids

A stop-motion video and corresponding still images of the formation of multiple NC-pyramids within the flat-top beam profile are shown in media 2 (multimedia online) and Fig. 5. Note that media 2 and Fig. 5 correspond to the same irradiated region as media 1 and Fig. 1 at a lower magnification in order to enable the observation of multiple NC-pyramids. Precursor cones develop at various ablation pulse counts and depths beneath the original surface. Regardless of the depth, precursor cone formation occurs from any of the theories for varied ablation thresholds previously mentioned. Once a precursor cone forms, the NC-pyramid develops through the second phase as is illustrated well in multimedia 2. The markers 1 and 2 indicate two NC-pyramids that form at different ablation pulse counts. Note that the NC-pyramid marked 1 is the same structure documented in Fig. 1. At large ablation pulse counts, the ablation crater is covered in a number of NC-pyramids with the size of each depending on the pulse count at which formation began. This variation in ablation pulse count for the onset of pyramid formation results in the peaks of the NC-pyramids at different

Table 1
Summary of shot by shot growth of NC-pyramids.

Phase I (~1–1000 pulses) Development of precursor cones	Phase II (~1000+ pulses) Development of nanoparticle covered pyramids
Nanoripples with a period ~600 nm; also known as laser induced periodic surface structures (LIPSS).	Part A: Geometric effects lead to preferential ablation of the base of the cones and the cones are etched into the surface with the same aspect ratio.
Precursor cones develop from a localized increase in the ablation threshold (from impurities, localized crystalline defects, or redeposition of material) (~500–1000 pulses).	Part B: Nanoparticles produced during the ablation process redeposit on the surface of the pyramid, eventually covering the entire pyramid.
Precursor cones continue to develop at various depths (pulse counts) in the surface (~1000+ pulses).	Once the nanoparticle layer covers the entire structure, growth of the NC-pyramid continues and layers of nanoparticles continuously build up on the outside of the structure.

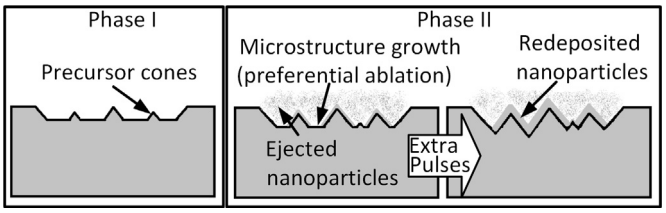

Fig. 6. Diagram of the two phases of NC-pyramid formation.

heights relative to the original surface. However, once formed, the location of the peak of a pyramid does not change. The NC-pyramids continue to grow larger due to preferential ablation and nanoparticle redeposition until they collide with neighboring NC-pyramids. Eventually the entire crater is filled with NC-pyramids (not shown here) and the formation process is halted.

3.2. Summary of the growth mechanisms for NC-pyramids

A summary of the shot-by-shot development of the NC-pyramids is described in Table 1 and diagrammed schematically in Fig. 6. The overall formation process is dominated by preferential ablation of micrometer-scale pyramids and the redeposition of nanoparticles created during the ablation process on top of those pyramids.

4. Conclusion

In this paper, the fabrication of NC-pyramids using femtosecond laser surface processing at laser fluence values near the ablation threshold has been demonstrated for the first time. Furthermore, the formation dynamics have been explained through the use of high-resolution stop-motion SEM videos. These unique NC-pyramid structures form at a fluence very close to the ablation threshold through a combination of preferential ablation and redeposition of nanoparticles created during the ablation process. NC-pyramids are characterized by micrometer-scale structures with an aspect ratio of roughly 1:1 that are covered in layers of nanoparticles. The attachment of these nanoparticles to the original cone structure is affected by the beam profile and whether the sample is in motion during processing; rastering with a Gaussian profile over a square flat-top profile results in multiple shells of nanoparticles, while stationary ablation creates pyramids with a single shell of nanoparticles. The structures reported in this paper have a different geometry and develop through different processes than any other FLSP structures previously published. Although the current work only presents results on Ni, similar structures have been observed to form on stainless steel (type 316, 304, and 430).

Acknowledgments

This work has been supported by a Multi-University Research Initiative (MURI) No. – W911NF-06-1-0446, Grant Assistance in Areas of National Need (GAANN) No. – P200A070344, and a grant through the Nebraska Center for Energy Sciences Research (NCESR) with funds provided by Nebraska Public Power District (NPPD) to the University of Nebraska-Lincoln (UNL) No. 4200000844.

Appendix A. Supplementary data

Supplementary data associated with this article can be found, in the online version, at http://dx.doi.org/10.1016/j.apsusc.2013.07.002.

References

[1] V.V. Iyengar, B.K. Nayak, M.C. Gupta, Optical properties of silicon light trapping structures for photovoltaics, Sol. Energy Mater. Sol. Cells 94 (2010) 2251–2257.
[2] B.K. Nayak, M.C. Gupta, K.W. Kolasinski, Spontaneous formation of nanospiked microstructures in germanium by femtosecond laser irradiation, Nanotechnology 18 (2007) 195302.
[3] J. Bonse, S. Baudach, J. Krüger, W. Kautek, M. Lenzner, Femtosecond laser ablation of silicon-modification thresholds and morphology, Appl. Phys. A: Mater. Sci. Process. 74 (2002) 19–25.
[4] K.W. Kolasinski, D. Mills, M. Nahidi, Laser assisted and wet chemical etching of silicon nanostructures, J. Vac. Sci. Technol. A: Vac., Surf. Films 24 (2006) 1474.
[5] A.Y. Vorobyev, C. Guo, Femtosecond laser structuring of titanium implants, Appl. Surf. Sci. 253 (2007) 7272–7280.
[6] V. Zorba, N. Boukos, I. Zergioti, C. Fotakis, Ultraviolet femtosecond, picosecond and nanosecond laser microstructuring of silicon: structural and optical properties, Appl. Opt. 47 (2008) 1846–1850.
[7] J. Zhu, G. Yin, M. Zhao, D. Chen, L. Zhao, Evolution of silicon surface microstructures by picosecond and femtosecond laser irradiations, Appl. Surf. Sci. 245 (2005) 102–108.
[8] V. Zorba, I. Alexandrou, I. Zergioti, A. Manousaki, C. Ducati, A. Neumeister, et al., Laser microstructuring of Si surfaces for low-threshold field-electron emission, Thin Solid Films 453-454 (2004) 492–495.
[9] T. Yong Hwang, C. Guo, Polarization and angular effects of femtosecond laser-induced conical microstructures on Ni, J. Appl. Phys. 111 (2012) 083518.
[10] B.K. Nayak, M.C. Gupta, K.W. Kolasinski, Formation of nano-textured conical microstructures in titanium metal surface by femtosecond laser irradiation, Appl. Phys. A: Mater. Sci. Process. 90 (2007) 399–402.
[11] B.K. Nayak, M.C. Gupta, Ultrafast laser-induced self-organized conical micro/nano surface structures and their origin, Opt. Laser Eng. 48 (2010) 966–973.
[12] T.H. Her, R.J. Finlay, C. Wu, E. Mazur, Femtosecond laser-induced formation of spikes on silicon, Appl. Phys. A: Mater. Sci. Process. 70 (2000) 383–385.
[13] B.R. Tull, J.E. Carey III, E. Mazur, J.P. McDonald, S.M. Yalisove, Silicon surface morphologies after femtosecond laser irradiation, MRS Bull. 31 (2011) 626–633.
[14] C.H. Crouch, J.E. Carey III, J.M. Warrender, M.J. Aziz, E. Mazur, F.Y. Génin, Comparison of structure and properties of femtosecond and nanosecond laser-structured silicon, Appl. Phys. Lett. 84 (2004) 1850.
[15] C.A. Zuhlke, T.P. Anderson, D.R. Alexander, Formation of multiscale surface structures on nickel via above surface growth and below surface growth mechanisms using femtosecond laser pulses, Opt. Express 21 (2013) 8460–8473.
[16] O. Auciello, R. Kelly, R. Iricibar, New insight into the development of pyramidal structures on bombarded copper surfaces, Radiat. Eff. 46 (1980) 105–117.
[17] P.E. Dyer, S.D. Jenkins, J. Sidhu, Development and origin of conical structures on XeCl laser ablated polyimide, Appl. Phys. Lett. 49 (1986) 453.
[18] D.J. Krajnovich, J.E. Vazquez, Formation of 'intrinsic' surface defects during 248 nm photoablation of polyimide, J. Appl. Phys. 73 (1993) 3001.
[19] R.S. Taylor, K.E. Leopold, D.L. Singleton, G. Paraskevopoulos, R.S. Irwin, The effect of debris formation on the morphology of excimer laser ablated polymers, J. Appl. Phys. 64 (1988) 2815.
[20] D.J. Krajnovich, J.E. Vazquez, R.J. Savoy, Impurity-driven cone formation during laser sputtering of graphite, Science 259 (2012) 1590–1592.
[21] C.A. Zuhlke, D.R. Alexander, J.C. Bruce III., N.J. Ianno, C.A. Kamler, W. Yang, Self assembled nanoparticle aggregates from line focused femtosecond laser ablation, Optics Express. 18 (2010) 4329–4339.
[22] R. Le Harzic, N. Huot, E. Audouard, C. Jonin, P. Laporte, S. Valette, et al., Comparison of heat-affected zones due to nanosecond and femtosecond laser pulses using transmission electronic microscopy, Appl. Phys. Lett. 80 (2002) 3886.
[23] S. Amoruso, R. Bruzzese, X. Wang, N.N. Nedialkov, P.A. Atanasov, Femtosecond laser ablation of nickel in vacuum, J. Phys. D: Appl. Phys. 40 (2007) 331–340.
[24] B. Wu, M. Zhou, J. Li, X. Ye, G. Li, L. Cai, Superhydrophobic surfaces fabricated by microstructuring of stainless steel using a femtosecond laser, Appl. Surf. Sci. 256 (2009) 61–66.
[25] N.G. Semaltianos, W. Perrie, P. French, M. Sharp, G. Dearden, K.G. Watkins, Femtosecond laser surface texturing of a nickel-based superalloy, Appl. Surf. Sci. 255 (2008) 2796–2802.
[26] B.K. Nayak, M.C. Gupta, Self-organized micro/nano structures in metal surfaces by ultrafast laser irradiation, Opt. Laser Eng. 48 (2010) 940–949.